Evaluation of Stress-strain Curve Estimates in Dynamic Experiments

Dirk Mohr, Gérard Gary, Bengt Lundberg

Evaluation of stress–strain curve estimates in dynamic experiments

Dirk Mohr [a,b,*], Gérard Gary [a], Bengt Lundberg [a,c]

[a] Solid Mechanics Laboratory (CNRS-UMR 7649), E´cole Polytechnique, 91128 Palaiseau, France
[b] Impact and Crashworthiness Laboratory, Massachusetts Institute of Technology, Cambridge, MA 02139, USA [c] The Angstro¨m Laboratory, Uppsala University, Box 534, SE-75121, Sweden

Accurate measurements of the forces and velocities at the boundaries of a dynamically loaded specimen may be obtained using split Hopkinson pressure bars (SHPB) or other experimental devices. However, the determination of a representative stress–strain curve based on these measurements can be challenging. Due to transient effects, the stress and strain fields are not uniform within the specimen. Several formulas have been proposed in the past to estimate the stress–strain curve from dynamic experiments. Here, we make use of the theoretical solution for the waves in an elastic specimen to evaluate the accuracy of these estimates. It is found that it is important to avoid an artificial time shift in the processing of the experimental data. Moreover, it is concluded that the combination of the output force based stress estimate and the average strain provides the best of the commonly used stress–strain curve estimates in standard SHPB experiments.

1. Introduction

Split Hopkinson Pressure Bar (SHPB) systems are commonly used to investigate the mechanical behavior of materials at high strain rates. The widespread use of SHPB systems in experimental dynamics is mainly due to the simplicity of the experimental procedure. The experimental technique is based on the early work of Hopkinson [1], who recorded a pressure-pulse profile using a slender bar. This approach has been widely adopted since the critical study of Davies [2]. The practical configuration consisting of a short specimen sandwiched between two slender bars is due to Kolsky [3]. High impedance bars made of steel are typically employed to perform dynamic experiments on metals. After being initially developed for compression tests, the technique was soon extended to tensile loading by Harding et al. [4] and to torsion loading by Duffy et al. [5]. To improve the accuracy of the measurements, wave dispersion effects in elastic and viscoelastic bars have been studied extensively (e.g. Davis [2], Yew and Chen [6], Follansbee and Franz [7], and Gorham [8], Gamby and Chaoufi [9], Wang et al. [10], Zhao and Gary [11], Liu and Subhash [12]). Other aspects involving the specimen response with regard to three-dimensional effects (e.g. Davies and Hunter [13], Dharan and Hauser [14], Bertholf and Karnes [15], Malinowski and Klepazko [16]) and transient effects (e.g. Lindholm [17], Conn [18], Bell [19], and Jahsman [20]) have also been investigated.

A comprehensive review of developments in SHPB testing has been provided in the ASM Handbook [21]. Over the past two decades, there has also been growing interest in testing soft materials using viscoelastic low-impedance bars made of polymeric materials (e.g. Gary et al. [22], Zhao and Gary [23], Sogabe et al. [24], Sawas et al. [25]). Gray III and Blumenthal [26] have reviewed the SHPB testing of soft materials. The main aspects that determine the accuracy of measurements in SHPB compression tests can be classified in two types. Firstly, there are aspects related to the accuracy of the forces and velocities at the specimen boundaries provided by the SHPB system. These global quantities can be obtained from the recorded wave signals without consideration of the specimen. Aspects of the second type are related to assumptions concerning the bar-specimen interaction and the specimen behavior: interface friction, lateral inertia of the specimen, uniaxial stress distribution, and stress equilibrium.

The present paper focuses on the estimation of the stress–strain curve, which involves aspects of the second type. A common feature of most static material tests is the existence of a zone within the specimen, the so-called gage section, in which the stress and strain fields can be considered uniform. The same conceptual approach is taken in dynamic materials testing. However, due to the presence of waves in dynamic experiments, both the stress and strain fields within a specimen are seldom uniform. A dynamic material test should be designed such as to minimize this inherent non-uniformity, a condition which is typically associated with

* Corresponding author. Impact and Crashworthiness Laboratory, Massachusetts Institute of Technology, Cambridge, MA 02139, USA.
E-mail address: mohr@mit.edu (D. Mohr).

"quasi-static equilibrium". However, when testing purely elastic materials such as brittle ceramics or low-impedance materials, the validity of this assumption needs to be checked with care (e.g. Ravichandran and Subhash [27], Song and Chen [28]). Before computers became generally available, the assumption of quasi-static equilibrium of the specimen had a special importance from a data processing point of view. This assumption allowed the measured data to be processed through real time analog integration (e.g. Kolsky [3]), and the stress–strain curve could be plotted in real time on an oscilloscope with a lasting image. This analog processing procedure required identical input and output bars, dispersion-free wave propagation in the bars as well as equilibrium of the specimen. Also, the distance between the strain gage and the specimen needed to be the same for the input and output bars.

With the general availability of numerical data acquisition and computer systems, most limitations associated with analog data processing could be overcome. For instance, the input and output bars no longer need to be identical; the waves do not need to be dispersion-free and different strain gage positions may be chosen on the input and output bars. Furthermore, two independent force measurements may be obtained (so-called input and output force) which allow the evaluation of the validity of the assumption of quasi-static equilibrium. Knowing that specimen equilibrium is never achieved exactly, we seek the best of the commonly used stress–strain curve estimates in a SHPB experiment. In the present paper, we therefore evaluate the accuracy of some widely used stress–strain curve estimates. The time shift of the waves is found to play a critical role as far as the accuracy is concerned. More specifically, it is found that the omission of artificial time shifts provides the best stress–strain curve estimates. In other words, once the force and displacement histories are known at the specimen boundaries, accurate estimates of the stress–strain curves should be made without further shifting the signals on the time axis.

This study is inspired by the processing of the experimental measurements obtained from compression tests. However, it is emphasized that we consider the SHPB apparatus as a device which allows us to obtain the forces and displacements at the boundaries of a dynamically loaded specimen. Therefore, parts of our analysis are relevant also for other testing systems in dynamics, for example systems combining the use of quartz load cells and digital image correlation based displacement measurements. Furthermore, all conclusions apply to dynamic compression, tension and torsion tests.

2. Preliminaries

In our discussion, we distinguish between "waves" and "time histories"[1]. A wave is represented by a function that depends on both the spatial coordinate x and time t. A time history on the other hand is a function that depends on time only. For example, if a wave described by the function passes by the point $x = x^*$ in space, we call the function $\varepsilon^*(t) = \varepsilon(x^*, t)$ a time history associated with this wave. The wave may be reconstructed from $\epsilon^*(t)$, but this requires further knowledge of the mechanical system.

Frequently, relations will be expressed in frequency space. We denote the Fourier transform of a time-dependent function $f(t)$ by $\widehat{f}(\omega)$, with the transformation relationships $\widehat{f}(\omega) = 1/2\pi \int_{-\infty}^{\infty} f(t) e^{-i\varpi t} \mathrm{d}t$ and $f(t) = \int_{-\infty}^{\infty} \widehat{f}(\omega) e^{i\varpi t} \mathrm{d}\omega$, where ω denotes the angular frequency. We recall here that the Fourier transforms of the time derivative of $f(t)$ and of the delayed function $f(t-a)$ are $i\omega\widehat{f}(\omega)$ and $e^{-i\omega a}\widehat{f}(\omega)$, respectively.

[1] As the word "history" implies the notion of "time", we frequently use the term "history" instead of "time history" in the sequel of this manuscript.

2.1. Split Hopkinson pressure bar compression test

Fig. 1 shows a schematic of a standard SHPB compression test. A cylindrical specimen is placed between the input and output bars. When a striker hits the free end of the input bar, a compressive strain wave is generated in this bar (the incident wave $\varepsilon_i(x,t)$). When reaching the input bar/specimen interface, this wave is partially transmitted and partially reflected towards the input bar/striker interface (the reflected wave $\varepsilon_r(x,t)$). When the compressive wave inside the specimen reaches the specimen/output bar interface, it is partially reflected and partially transmitted into the output bar (the transmitted wave $\varepsilon_t(x,t)$).

In addition to loading and supporting the specimen, the input and output bars are used to obtain accurate force and displacement history measurements at the bar/specimen interfaces. Based on strain history recordings at selected positions on the input and output bars, the strain waves within the bars are reconstructed and used to calculate the force and displacement histories at the bar/specimen interfaces. Subsequently, a stress–strain curve is estimated for the material of the specimen. As mentioned, the SHPB procedure involves key assumptions regarding:

(1) Dispersion in the bars. The shapes and amplitudes of the waves traveling in the bars may change due to geometric and material dispersion. It is important to take these effects into account when calculating the strain histories at the bar/specimen interfaces based on strain history measurements at different locations.
(2) Separation of the waves in the input bar. The strain history in the input bar is typically measured near the center of the bar to avoid the superposition of the incident and reflected waves at the measurement location. Unless signal deconvolution techniques are used, it is important to verify that the incident wave has ceased before the appearance of the reflected wave.
(3) Planarity of the bar/specimen contact surfaces. The diameter of the specimen is typically smaller than those of the input and output bars. Thus, the compressive loading of the specimen may result in local indentations of the input and output bars. In other words, the bar surfaces do not remain flat which reduces the accuracy of the interface displacement predictions based on 1-D wave propagation theory for cylindrical bars.
(4) Correction for radial inertia and interface friction. Except for materials with Poisson's ratio zero, the diameter of a cylindrical specimen changes during a compression test. As a result, radial inertia effects on the specimen level may come into play. Correction formulas have been developed in the past to correct for both radial inertia and bar/specimen interface friction. However, most dynamic compression specimens are designed to make both effects small.
(5) Shifting of the waves. Due to the axial inertia and stiffness of the specimen, the force histories at the bar/specimen interfaces are not identical. Only in the case of quasi-static equilibrium, these differences become negligibly small. It is common practice to artificially shift the waves on the time axis to decrease the difference between the input and output force histories. In most experiments, the effect of shifting is more pronounced at small strains than at large strains.

As discussed by Subhash and Ravichandran [29] in the context of SHPB testing of ceramics, additional assumptions regarding state of stress and strain within the specimen may be necessary.

2.2. Measurement and reconstruction of the waves in the SHPB system

Strain measurements on the bar surfaces are typically used to determine the strain waves in a SHPB system. Such measurements

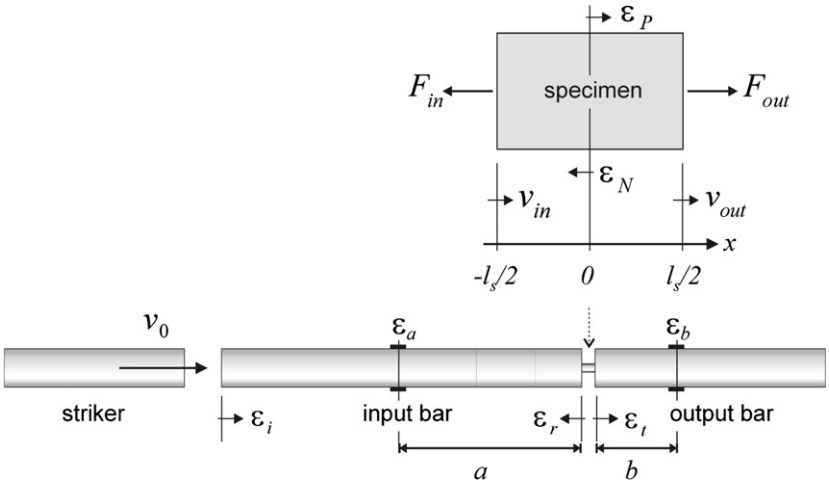

Fig. 1. Schematic of conventional SHPB test set-up with detail of specimen. The input and output bar strain gages are positioned at a distance of a and b from the respective specimen/bar interfaces.

only provide the surface strain as a function of time at a particular location $x = x^*$ along the bar axis, $\varepsilon^*(t) = \varepsilon(x^*, t)$. However, if the measured strain history is associated with a single wave of known propagation direction, three-dimensional single mode wave propagation theory may be used to reconstruct the full wave as a function of time and space. Using the Fourier transform of the measured strain history $\widehat{\epsilon}^*(\omega)$, we have the reconstructed wave

$$\varepsilon(x,t) = \int_{-\infty}^{\infty} \widehat{\varepsilon}^*(\omega) e^{i\gamma\xi(x-x^*)} e^{i\varpi t} \mathrm{d}\omega, \tag{1}$$

where $\gamma = -1(\gamma = 1)$ for a wave traveling in the positive (negative) x-direction. The complex wave number is defined as $\xi(\omega) = \omega/c(\omega) - i\alpha_d(\omega)$, where the functions $c(\omega) > 0$ and $x = l_s/2$ represent the phase velocity and the damping, respectively. In a 3-D context, both functions depend on the bar diameter as well as the viscoelastic bar material properties.

Using Eq. (1), we may reconstruct the incident and reflected waves in the input bar and then evaluate the corresponding strain histories at the input bar/specimen interface. If $\varepsilon_a(t)$ is the strain history recorded by a strain gage positioned at a distance a from the specimen interface, the Fourier transform of the strain history $\varepsilon_i(t)$ associated with the incident wave at the input bar/specimen interface is represented by

$$\widehat{\varepsilon}_i(\omega) = \widehat{\varepsilon}_a(\omega) e^{-i\xi_a a}. \tag{2}$$

Analogously, the strain history $\varepsilon_r(t)$ associated with the reflected wave at the input bar/specimen interface is represented by

$$\widehat{\varepsilon}_r(\omega) = \widehat{\varepsilon}_a(\omega) e^{i\xi_a a}. \tag{3}$$

These relations hold true only if there is no superposition of the incident and reflected waves at the location of the strain gage.

In the output bar, the strain history associated with the transmitted wave at the specimen interface is given by

$$\widehat{\varepsilon}_t(\omega) = \widehat{\varepsilon}_b(\omega) e^{i\xi_b b}, \tag{4}$$

where $\varepsilon_b(t)$ is the strain history measured at a distance b from the output bar/specimen interface. Different subscripts have been used for the wave numbers ξ in the input and output bars to highlight that these may be made of different materials and/or have different diameters. It is emphasized that all strain histories are defined on the same time axis t.

Fig. 2a shows an example of strain history recordings in a SHPB experiment. At the input bar strain gage location, we record the strain histories associated with the incident and reflected waves. Similarly, at the output bar strain gage location, we record the strain history associated with the transmitted wave. Fig. 2b shows the strain histories at the bar/specimen interfaces. On the time axis, the incident wave strain history at the input bar/specimen interface shows non-zero values later than at the strain gage position. Conversely, the strain history associated with the reflected wave rises earlier to non-zero values. The same applies to the strain histories associated with the transmitted wave in the output bar.

2.3. Forces and velocities at the bar/specimen interfaces

Based on the strain histories at the bar/specimen interfaces, the forces acting on the specimen as well as the interface velocities may be calculated using 1 D theory. At the input bar/specimen interface, the contact force and the interface velocity are

$$F_{\mathrm{in}}(t) = c_i Z_i [\varepsilon_i(t) + \varepsilon_r(t)], \tag{5}$$

$$v_{\mathrm{in}}(t) = c_i [-\varepsilon_i(t) + \varepsilon_r(t)], \tag{6}$$

where $c_i = \sqrt{E_i/\rho_i}$ is the wave speed, $Z_i = E_i A_i / c_i$ is the characteristic impedance, A_i is the cross-sectional area, E_i is the Young's modulus, and ρ_i is the mass density. Similarly, we have the contact force and the velocity at the output bar/specimen interface,

$$F_{\mathrm{out}}(t) = c_o Z_o \varepsilon_t(t), \tag{7}$$

$$v_{\mathrm{out}}(t) = -c_o \varepsilon_t(t). \tag{8}$$

The characteristic impedance of the output bar, Z_o, is defined by the corresponding output bar properties A_o, E_o and ρ_o. The forces are defined as positive in tension, while the velocities are defined as positive in the positive direction of the x-axis.

2.4. Wave propagation in an elastic specimen

In the previous subsection, we expressed the interface forces and velocities in terms of the waves in the input and output bars. In the case of an elastic specimen, the interface forces and velocities may also be expressed in terms of the waves inside the specimen.

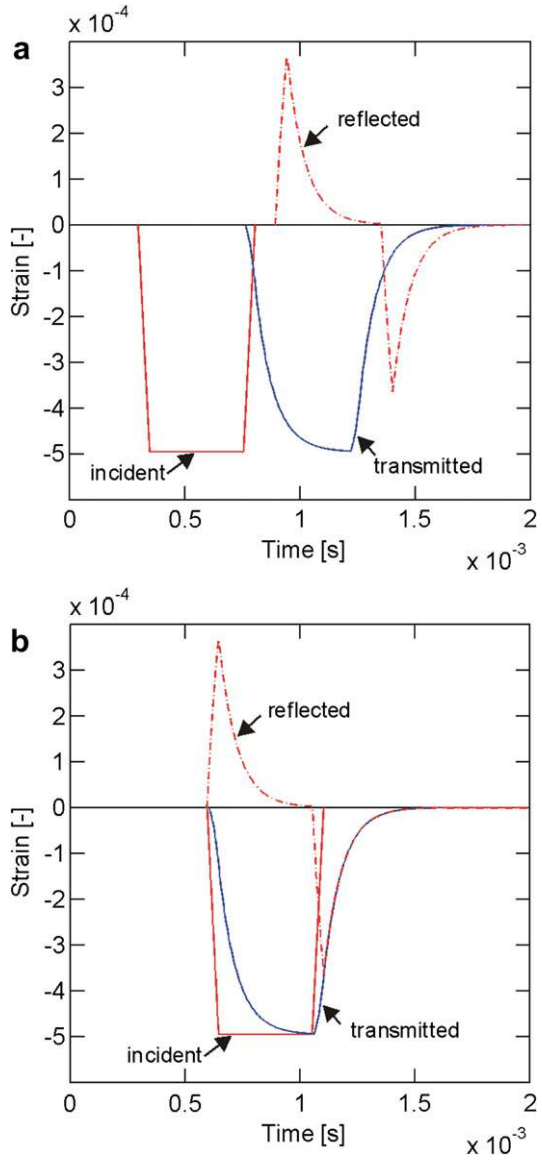

Fig. 2. Strain histories of the incident wave (solid red line), the reflected wave (dashed red line) and the transmitted wave (solid blue line) at different locations in the input bar (red curves) and output bar (blue curves): (a) at the positions of the strain gages, (b) at the bar/specimen interfaces. (For interpretation of the references to colour in this figure legend, the reader is referred to the web version of this article).

These relationships are obtained from the solution of the wave equation within the specimen. Consider a cylindrical specimen of length l_s, cross-sectional area A_s, Young's modulus E_s, mass density ρ_s, wave speed $c_s = \sqrt{E_s/\rho_s}$, and characteristic impedance $Z_s = A_s E_s/c_s$. As illustrated in Fig. 1, we define the origin of the spatial coordinate system at the center of the specimen. Following Mousavi et al. [29], we write the strain in the specimen as

$$\widehat{\varepsilon}(x,\omega) = \widehat{\varepsilon}_P(\omega)e^{-i\omega x/c_s} + \widehat{\varepsilon}_N(\omega)e^{i\omega x/c_s}, \tag{9}$$

where $\widehat{\varepsilon}_P(\omega)$ and $\widehat{\varepsilon}_N(\omega)$ are the strains associated with the rightward and leftward traveling waves at the mid-section of the specimen. Thus, the force and velocity at the input bar/specimen interface ($x = -l_s/2$) read

$$\widehat{F}_{\text{in}}(\omega) = c_s Z_s\Big[\alpha\widehat{\varepsilon}_P(\omega) + \beta\widehat{\varepsilon}_N(\omega)\Big], \tag{10}$$

$$\widehat{v}_{\text{in}}(\omega) = c_s\Big[-\alpha\widehat{\varepsilon}_P(\omega) + \beta\widehat{\varepsilon}_N(\omega)\Big], \tag{11}$$

with

$$\alpha(\omega) = e^{i\omega t_s/2}, \quad \beta(\omega) = e^{-i\omega t_s/2} \tag{12}$$

where $t_s = l_s/c_s$ denotes the transit time for an elastic wave propagating through the specimen. Analogously, we have the force and velocity at the output bar/specimen interface ($x = l_s/2$),

$$\widehat{F}_{\text{out}}(\omega) = c_s Z_s\Big[\beta\widehat{\varepsilon}_P(\omega) + \alpha\widehat{\varepsilon}_N(\omega)\Big], \tag{13}$$

$$\widehat{v}_{\text{out}}(\omega) = c_s\Big[-\beta\widehat{\varepsilon}_P(\omega) + \alpha\widehat{\varepsilon}_N(\omega)\Big]. \tag{14}$$

In a SHPB compression experiment, the output bar may be considered semi-infinite (between the strain gage location and the output bar/specimen interface, there are only waves traveling away from the specimen during the interval of measurement). Thus, the output force

$$\widehat{F}_{\text{out}}(\omega) = -Z_o\widehat{v}_{\text{out}}(\omega) \tag{15}$$

is directly proportional to the output velocity $\widehat{v}_{\text{out}}(\omega)$. Introducing this relation in Eqs. (13) and (14), we find for the frequency-dependent ratio of the two strain waves inside the specimen,

$$\frac{\widehat{\varepsilon}_N(\omega)}{\widehat{\varepsilon}_P(\omega)} = \text{Re}^{-i\omega t_s}, \tag{16}$$

where $R = (Z_o - Z_s)/(Z_o + Z_s)$. It is worth noting that this ratio does not depend on the impedance of the input bar. Eq. (16) is valid for SHPB systems with different input and output bars.

3. Stress–strain curve estimates

Even though the forces and velocities at the boundaries of a dynamically loaded specimen can be determined to a high degree of accuracy, it can be difficult to determine the stress–strain curve from such data. Under static loading conditions, both the stresses and strains are uniform within cylindrical specimens. However, in a dynamic experiment, the stress and strain fields are non-uniform. As the stress and strain field variations are a priori unknown, exact stress and strain calculations need to be substituted by estimates. The challenge is to come up with accurate estimates of the stress history $\sigma(t)$ and the corresponding strain history $\varepsilon(t)$ such that their combination

$$\sigma(\varepsilon) = \sigma(t)\circ\varepsilon^{-1}(t) \tag{17}$$

provides an accurate estimate of the stress–strain curve $\sigma(\varepsilon)$ of the dynamically tested material. In the following, we investigate estimates that are widely used.

3.1. Direct estimates

The spatial average of the axial strain field within the specimen is chosen to estimate the strain history. It can be expressed in terms of the interface velocities $v_{\text{in}}(t)$ and $v_{\text{out}}(t)$ as

$$\varepsilon^{de}_{av}(t) = \frac{1}{l_s}\int_{-l_s/2}^{l_s/2}\varepsilon(x,t)\mathrm{d}x = \frac{1}{l_s}\int_0^t[v_{\text{out}}(t) - v_{\text{in}}(t)]\mathrm{d}t, \tag{18}$$

and correspondingly

$$\widehat{\varepsilon}^{de}_{av}(\omega) = \frac{1}{i\omega l_s}\Big[\widehat{v}_{\text{out}}(\omega) - \widehat{v}_{\text{in}}(\omega)\Big]. \tag{19}$$

It is not possible to express the spatial average of the stress field in a similar manner. Instead, two distinct stress-time history estimates are considered. Firstly, the stress is estimated as the average of the forces at the input and output bar/specimen interfaces (which is not the same as the spatial average of the stress field), i.e.

$$\sigma_{av}^{de}(t) = \frac{F_{\text{in}}(t) + F_{\text{out}}(t)}{2A_s}. \tag{20}$$

In most standard SHPB experiments, we have a compressive incident wave and a tensile reflected wave. Thus, in terms of absolute measurements, the input force is determined from the difference of two strain history measurements (see Eq. (5)). As a result, the corresponding standard uncertainty in the input force measurement is usually higher than that of the output force which is directly proportional to the strain history of the transmitted wave (cf. Grolleau et al. [30]). Therefore, as an alternative to Eq. (20), the stress is frequently estimated based on the output force history only, i.e.

$$\sigma_{\text{out}}^{de}(t) = \frac{F_{\text{out}}(t)}{A_s}. \tag{21}$$

Combining these two stress estimates with the average strain estimate yields two direct estimates of the stress–strain curve. These two estimates are called "direct estimates" as the original force and velocity measurements have not been artificially shifted on the time axis before calculating the stress–strain curve. In other words the force and velocity histories at the specimen interfaces are directly used to obtain the stress–strain curve.

3.2. Foot-shifting

To simplify the processing of SHPB measurements, the original measurement data are sometimes modified using a procedure which we refer to as "foot-shifting". The idea is to shift the strain history associated with the transmitted wave on the time axis such that it rises to non-zero values at the same time as the incident and reflected waves at the input bar/specimen interface. This procedure is illustrated in Fig. 3 which magnifies a detail of Fig. 2b. The "foot" of the transmitted strain history indicates the point on the time axis where the strain changes for the first time from zero to a non-zero value. If the incident and reflected waves in the input bar have been reconstructed correctly (which requires consideration of dispersion), the corresponding "foots" of the strain-time histories of the incident and reflected waves at the input bar/specimen interface will coincide. However, the transmitted wave at the output bar/specimen interface is delayed by the transit time $t_s = l_s/c_s$ of an elastic wave traveling through the specimen. When using the foot-shifting procedure, the strain history associated with the transmitted wave is shifted on the time axis such that its "foot" coincides with that of the strain histories at the input bar/specimen interface.

Formally, the foot-shifting estimates may be written as follows. The average strain in the specimen reads $\varepsilon_{av}^{fs}(t) = (1/l_s)\int_0^t [v_{\text{out}}(t+t_s) - v_{\text{in}}(t)]\mathrm{d}t$ which corresponds to

$$\widehat{\varepsilon}_{av}^{fs}(\omega) = \frac{1}{i\omega l_s}\left[\widehat{v}_{\text{out}}(\omega)e^{i\omega t_s} - \widehat{v}_{\text{in}}(\omega)\right]. \tag{22}$$

The corresponding stress estimate reads

$$\widehat{\sigma}_{\text{out}}^{fs}(\omega) = \frac{1}{A_s}\widehat{F}_{\text{out}}(\omega)e^{i\omega t_s}. \tag{23}$$

The foot-shifting procedure is particularly convenient when neglecting the wave dispersion in both the input and output bars. In this case, it is sufficient to identify the "foots" of all three waves in the strain histories which have been recorded at the strain gage locations and then shift these to the same position on the time axis in order to calculate the foot-shifted stress–strain curve estimates.

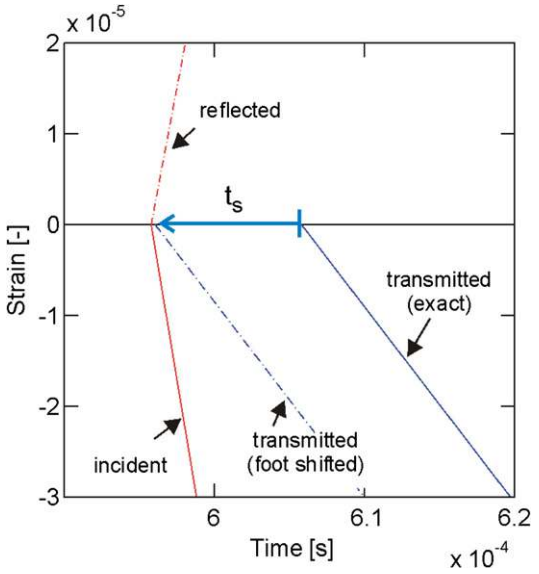

Fig. 3. Beginning of the strain histories at the bar/specimen interfaces (detail of Fig. 2b). The dashed blue line shows the strain history of the transmitted wave after shifting the beginning of this wave in time (so-called "foot-shifting") such that all strain histories begin simultaneously. (For interpretation of the references to colour in this figure legend, the reader is referred to the web version of this article).

3.3. Kolsky estimate

In the present context, the term "Kolsky estimate" is used to refer to one particular type of estimate that is based on assumptions presented in Kolsky [3]. Kolsky proposed his formulas before computers had become generally available for data processing. He used identical input and output bars (same length, diameter and material) and put strain gages at the center of each bar. Neglecting the dispersion in the bars and assuming quasi-static equilibrium, Kolsky assumed

$$\widehat{\varepsilon}_i(\omega) + \widehat{\varepsilon}_r(\omega) \cong \widehat{\varepsilon}_t(\omega), \tag{24}$$

to estimate the strain as

$$\widehat{\varepsilon}_{\text{Ko}}(\omega) = -\frac{2c_o}{i\omega l_s}\widehat{\varepsilon}_r(\omega). \tag{25}$$

In terms of the force and velocity at the input specimen/bar interface, this strain estimate becomes

$$\widehat{\varepsilon}_{\text{Ko}}(\omega) = \frac{1}{i\omega l_s}\left[-\frac{\widehat{F}_{\text{in}}(\omega)}{Z_o} - \widehat{v}_{\text{in}}(\omega)\right]. \tag{26}$$

At the same time, Kolsky used the output force to estimate the stress-time history. In other words, Kolsky's stress estimate is the same as the output force based direct stress estimate (21). It is worth noting that the prescription of quasi-static equilibrium by Eq. (24) involves some implicit "foot-shifting".

3.4. Summary

In summary, we consider four distinct stress–strain curve estimates:

(i) Direct estimate, average force based stress and average strain:

$$\sigma_{\mathrm{I}}(\varepsilon_{\mathrm{I}}) \;=\; \sigma^{de}_{av}(t) \circ \Big[\varepsilon^{de}_{av}(t)\Big]^{-1}. \tag{27}$$

(ii) Direct estimate, output force based stress and average strain:

$$\sigma_{\mathrm{II}}(\varepsilon_{\mathrm{II}}) \;=\; \sigma^{de}_{\mathrm{out}}(t) \circ \Big[\varepsilon^{de}_{av}(t)\Big]^{-1}. \tag{28}$$

(iii) Foot-shifted estimate, output force based stress and average strain:

$$\sigma_{\mathrm{III}}(\varepsilon_{\mathrm{III}}) \;=\; \sigma^{fs}_{\mathrm{out}}(t) \circ \Big[\varepsilon^{fs}_{av}(t)\Big]^{-1}. \tag{29}$$

(iv) Kolsky estimate, output force based stress and reflected wave based strain:

$$\sigma_{\mathrm{IV}}(\varepsilon_{\mathrm{IV}}) \;=\; \sigma^{de}_{\mathrm{out}}(t) \circ [\varepsilon_{\mathrm{Ko}}(t)]^{-1}. \tag{30}$$

Other combinations of the above estimates may be considered, e.g. evaluating Kolsky's estimate based on the foot-shifted signals, combining the average force based stress with the Kolsky strain, etc. For the clarity of our presentation, however, we limit ourselves to the above four estimates.

4. Evaluation

It is of interest to evaluate the stress–strain curve estimates in both the elastic and elastic–plastic range. Here, the evaluation is limited to the elastic case where the choice of estimate appears to have the greatest importance. In this case, the quality of the stress–strain curve estimates may be evaluated by comparing the apparent modulus $E(\omega)$ with the real modulus E_s of the elastic specimen material. Given the Fourier transform of the stress history $\widehat{\sigma}(\omega)$, and the strain-time history $\widehat{\epsilon}(\omega)$, we have the apparent complex modulus

$$E(\omega) \;=\; E'(\omega) + iE''(\omega) \;=\; \frac{\widehat{\sigma}(\omega)}{\widehat{\epsilon}(\omega)}, \tag{31}$$

where $E'(\omega)$ and $E''(\omega)$ denote the real and imaginary parts, respectively. For a perfect estimate, $E'(\omega)$ should be constant and equal the Young's modulus, $E'(\omega) = E_s$, while the imaginary part should be zero, $E''(\omega) = 0$.

4.1. Direct estimates

Using the elastic solution for the waves within the specimen (see Eqs. (11) and (14)), we write the average strain estimate (19) as

$$\widehat{\varepsilon}^{de}_{av} \;=\; \frac{1}{i\omega l_s}\Big[\widehat{v}_{\mathrm{out}} - \widehat{v}_{\mathrm{in}}\Big] \;=\; \frac{\alpha-\beta}{i\omega t_s}\Big(\widehat{\varepsilon}_P + \widehat{\varepsilon}_N\Big). \tag{32}$$

Also, by Eqs. (10) and (13), the average force based stress estimate (20) becomes

$$\widehat{\sigma}^{de}_{av} \;=\; \frac{1}{2}E_s(\alpha+\beta)\Big(\widehat{\varepsilon}_P + \widehat{\varepsilon}_N\Big). \tag{33}$$

Analogously, we may make use of the exact elastic solution for the waves within the specimen to express the output force based stress estimate as

$$\widehat{\sigma}^{de}_{\mathrm{out}} \;=\; E_s\Big(\beta\widehat{\varepsilon}_P + \alpha\widehat{\varepsilon}_N\Big). \tag{34}$$

Using the expressions for stress and strain above, we can now calculate the apparent complex moduli corresponding to the stress–strain curve estimates given by Eqs. (27) and (28). Combination of the average force based stress estimates with the average strain estimate yields the modulus estimate

$$E_{\mathrm{I}}(\omega) \;=\; \frac{\widehat{\sigma}^{de}_{av}}{\widehat{\varepsilon}^{de}_{av}} = \frac{1}{2}E_s i\omega t_s \frac{\alpha+\beta}{\alpha-\beta} \;=\; E_s\frac{\omega t_s/2}{\tan(\omega t_s/2)}. \tag{35}$$

Similarly, the modulus estimate based on the output force and the average strain becomes

$$E_{\mathrm{II}}(\omega) \;=\; \frac{\widehat{\sigma}^{de}_{\mathrm{out}}}{\widehat{\varepsilon}^{de}_{av}} \;=\; E_s e^{-i\omega t_s/2}\frac{\omega t_s/2}{\sin(\omega t_s/2)}\,\frac{1+R}{1+\mathrm{Re}^{-i\omega t_s}}. \tag{36}$$

4.2. Foot-shifting

As for the direct estimates, we make use of the exact theoretical solution for the waves inside the specimen to evaluate the foot-shifted estimates. Recall that the foot-shifting corresponds to a time shift of the strain history associated with the transmitted wave. Using Eqs. (11) and (14) in (22), we obtain the foot-shifting based average strain estimate

$$\widehat{\varepsilon}^{fs}_{av} \;=\; \frac{1}{i\omega t_s}\Big[\Big(-\beta\widehat{\varepsilon}_P + \alpha\widehat{\varepsilon}_N\Big)e^{i\omega t_s} + \alpha\widehat{\varepsilon}_P - \beta\widehat{\varepsilon}_N\Big]. \tag{37}$$

The output force based stress estimate reads

$$\widehat{\sigma}^{fs}_{\mathrm{out}} \;=\; E_s\Big(\beta\widehat{\varepsilon}_P + \alpha\widehat{\varepsilon}_N\Big)e^{i\omega t_s}. \tag{38}$$

Combining the strain and stress estimates, we get the corresponding foot-shifted modulus estimate

$$E_{\mathrm{III}}(\omega) \;=\; \frac{\widehat{\sigma}^{fs}_{\mathrm{out}}}{\widehat{\varepsilon}^{fs}_{av}} \;=\; \frac{E_s}{1-Z_s/Z_o}e^{i\omega t_s}\frac{\omega t_s}{\sin(\omega t_s)}. \tag{39}$$

4.3. Kolsky estimate

Using Kolsky's data processing procedure along with the exact elastic solution, the strain estimate reads

$$\widehat{\varepsilon}_{eq}(\omega) \;=\; \frac{1}{i\omega t_s}\Big[\alpha\widehat{\varepsilon}_P - \beta\widehat{\varepsilon}_N - \frac{Z_s}{Z_o}\Big(\alpha\widehat{\varepsilon}_P + \beta\widehat{\varepsilon}_N\Big)\Big]. \tag{40}$$

Recall that Kolsky used the output force based direct stress estimate (37). Hence, the modulus estimate reads

$$E_{\mathrm{IV}}(\omega) \;=\; \frac{\widehat{\sigma}^{de}_{\mathrm{out}}}{\widehat{\varepsilon}_{eq}} \;=\; \frac{E_s}{1-(Z_s/Z_o)^2}\,\frac{\omega t_s}{\sin(\omega t_s)}. \tag{41}$$

Note that Kolsky's formulas are applicable only to SHPB systems with identical input and output bar properties ($Z_i = Z_o$).

4.4. Evaluation

All modulus estimates depend on the normalized angular frequency ωt_s. This dimensionless number is small within the range of significant frequencies of a typical SHBP compression test. For example, when testing a $l_s = 5$ mm long steel or aluminum specimen, we have $t_s \cong 1\mu$s. At the same time, the maximum frequencies in a typical SHPB test are smaller than $\omega/2\pi < 100$kHz. Hence, we have $\omega t_s/2\pi \le 0.1$. In other words, the period of the wave of highest frequency is still at least ten times larger than the specimen transit time t_s. For evaluation purposes, we also calculate the second-order Taylor expansion of the estimated moduli:

(i) Direct estimate, average force based stress and average strain:

$$E_{\mathrm{I}}(\omega) \cong E_s\left[1 - \frac{1}{12}(\omega t_s)^2\right]. \tag{42}$$

(ii) Direct estimate, output force based stress and average strain:

$$E_{\mathrm{II}}(\omega) \cong E_s[1 - i(\omega t_s/2)Z_s/Z_o]. \tag{43}$$

(iii) Foot-shifted estimate, output force based stress and average strain:

$$E_{\mathrm{III}}(\omega) \cong \frac{E_s}{1 - Z_s/Z_0}(1 + i\omega t_s). \tag{44}$$

(iv) Kolsky estimate, output force based stress and reflected wave based strain:

$$E_{\mathrm{IV}}(\omega) \cong \frac{E_s}{1 - (Z_s/Z_o)^2}\left[1 + \frac{1}{6}(\omega t_s)^2\right]. \tag{45}$$

The strain and stress estimates are "in phase" when the imaginary part of the estimated modulus is zero. This is the case for the average force based direct estimate $E_{\mathrm{I}}(\omega)$ and the Kolsky estimate $E_{\mathrm{IV}}(\omega)$. The output force based direct estimate $E_{\mathrm{II}}(\omega)$ has a negative imaginary part for positive frequencies. This means that the stress lags the strain, which corresponds to a hypothetical material that delivers energy when subjected to harmonic loading. Conversely, the imaginary part of $E_{\mathrm{III}}(\omega)$ is positive for positive frequencies and the stress leads the strain. Thus, the foot-shifted estimate suggests a hypothetical material that absorbs energy.

Observe that all modulus estimates except for $E_{\mathrm{I}}(\omega)$ depend on the specimen-to-output bar impedance ratio Z_s/Z_o. This impedance ratio determines the magnitude of the ratio $\widehat{\varepsilon}_N/\widehat{\varepsilon}_P$ of the rightward and leftward traveling waves inside the specimen (see Eq. (16)). In the case of $Z_s/Z_o = 1$, there is no reflection within the specimen and hence $\widehat{\varepsilon}_N = 0$. For $Z_s/Z_o \to 0$, the specimen/output bar interface acts as a rigid boundary. Consequently, the leftward traveling wave $\widehat{\varepsilon}_N$ is equal to $\widehat{\varepsilon}_P$ with a delay of t_s. The evaluation of Eq. (16) yields

$$\lim_{Z_s/Z_o \to 0}\left(\frac{\widehat{\varepsilon}_N}{\widehat{\varepsilon}_P}\right) = e^{-i\omega t_s}. \tag{46}$$

It is worth noting that the output force based direct modulus estimate $E_{\mathrm{II}}(\omega)$ and the Kolsky estimate $E_{\mathrm{IV}}(\omega)$, Eqs. (36) and (41), respectively, are identical for $Z_s/Z_o \to 0$,

$$\lim_{Z_s/Z_o \to 0} E_{\mathrm{II}}(\omega) = \lim_{Z_s/Z_o \to 0} E_{\mathrm{IV}}(\omega) = E_s\frac{\omega t_s}{\sin(\omega t_s)}. \tag{47}$$

This can also be seen from Eqs. (19) and (26): the only difference between these two estimates is in the estimation of the output velocity; however, as the output velocity is zero for $Z_s/Z_o \to 0$, both estimates become identical. The real-valued Kolsky estimate $E_{\mathrm{IV}}(\omega)$ is monotonic in Z_s/Z_o. Thus, the greater the specimen/bar impedance mismatch (with $Z_s/Z_o < 1$), the smaller the error in the Kolsky modulus estimate.

In order to quantify the error in the stress–strain curve estimates, we define the normalized distance between the estimated complex modulus $E_i(\omega)$ and the true material modulus E_s

$$e_i = \frac{|E_i(\omega) - E_s|}{E_s}. \tag{48}$$

These error functions are depicted in Fig. 4 for two distinct impedance mismatches:

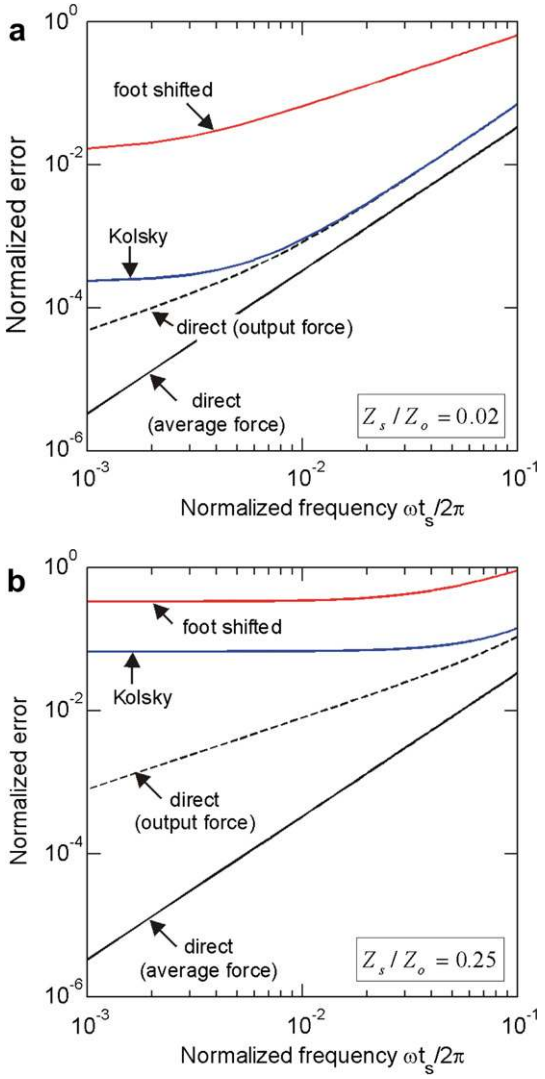

Fig. 4. Modulus errors as a function of the normalized angular frequency for different stress–strain curve estimates: (a) large impedance mismatch, (b) small impedance mismatch.

(i) Large impedance mismatch ($Z_s/Z_o = 0.02$, Fig 4a). This example corresponds to the testing of 10 mm diameter PMMA specimen in a 20 mm diameter steel bar system.

(ii) Small impedance mismatch ($Z_s/Z_o = 0.25$, Fig. 4b). This configuration corresponds to a 10 mm diameter steel specimen in a 20 mm diameter steel bar system.

Both plots show that the curves are in hierarchical order. The smallest error is observed for the average force based direct estimate $E_{\mathrm{I}}(\omega)$ while the error for the output force based estimate $E_{\mathrm{II}}(\omega)$ appears to be sandwiched between the curve for $E_{\mathrm{I}}(\omega)$ and the Kolsky estimate $E_{\mathrm{IV}}(\omega)$. The error of the foot-shifting based estimate $E_{\mathrm{III}}(\omega)$ is the largest among the present estimates. It is one to two orders of magnitude larger than the other estimates with an error of up to 100% at high frequencies. All error functions are monotonic with respect to the normalized frequency ωt_s. For the direct estimates, the error vanishes at low frequencies. As shown in Fig. 4 and by Eq. (45), the error of the Kolsky estimates does not vanish at low frequencies. The same holds true for the foot-shifted estimate where the error at low frequencies is still larger by a factor of Z_o/Z_s as compared to the Kolsky estimate. The curves in Fig. 4a also indicate the aforementioned convergence of the estimates $E_{\mathrm{II}}(\omega)$

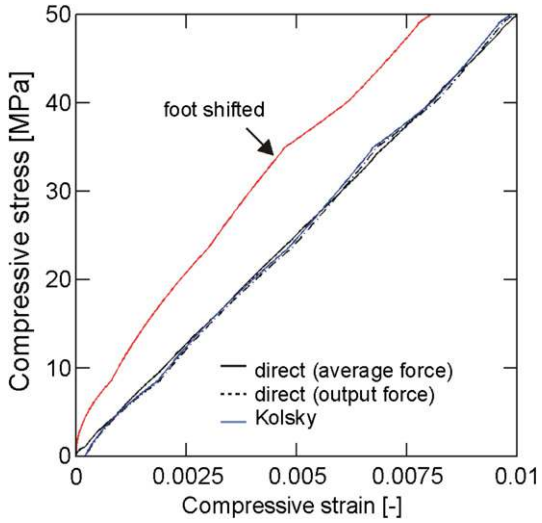

Fig. 5. Plot of the estimated stress–strain curves for a dynamic compression experiment on PMMA.

and $E_{\mathrm{IV}}(\omega)$ for large impedance mismatch. It is concluded from the evaluation of the modulus estimates, that all of them provide reasonable results except the foot-shifted one. Irrespective of the specimen/bar impedance mismatch and frequency, the foot-shifted estimate yields poor results for the stress–strain relationship.

5. Application and discussion

The previous evaluation of the stress–strain estimates has been carried out in the frequency domain. The extrapolation of the error estimates from the frequency domain into the time domain is not straightforward. In particular, the stress–strain curve $\sigma(\varepsilon) = \sigma(t) \circ \varepsilon^{-1}(t)$ is linear only if $E(\omega)$ is real and constant. In all other cases, this relationship is non-linear and the modulus needs to be estimated through linear interpolation of the measured stress–strain curve.

To illustrate the error in the different stress–strain curve estimates in the time domain, we performed a one-dimensional numerical simulation of a SHPB experiment on a PMMA specimen ($E_s = 5000$ MPa, $\rho_s = 1.2$ g/cm^2, $D_s = 20$ mm, $l_s = 20$ mm). The SHPB systems comprises of 20 mm diameter steel input and output bars ($E_b = 210$ GPa, $\rho_s = 7.8$ g/cm^3); the corresponding input and output strain gages are positioned at $a = 1505$ mm and $b = 800$ mm from the specimen/bar interfaces. We generated an incident wave with rise time 50 μs that imitates a striker impact at 5 m/s.

The strain histories at the strain gage locations associated with the incident, reflected and transmitted waves are depicted in Fig. 2a. The corresponding strain histories at the specimen/bar interfaces have been reconstructed in Fig. 2b. The strain signals just appear at different times since they have been evaluated at different locations. Subsequently, we evaluate the strain and stress history estimates according to the different formulas given in Section 4. Fig. 5 summarizes the corresponding stress–strain curves. The black solid line depicts the average force based direct stress estimate σ_{av}^{de} as a function of the average strain estimate ϵ_{av}^{de}. As predicted by the frequency space analysis, this curve provides the best representation of the response of the linear elastic material. The plot of the output force based direct stress estimate $\sigma_{\mathrm{out}}^{de}$ as a function of the average direct strain estimate (dashed line) also provides a good approximation of the linear stress–strain curve. The specimen-to-output bar impedance ratio is relatively small ($Z_s/Z_o = 0.06$). Consequently, the Kolsky estimate closely follows the output force based direct estimate, as predicted by the theoretical analysis in the frequency space. The plot of the foot-shifting based stress–strain curve confirms the conclusion of the theoretical analysis: the foot-shifted estimate provides the least accurate representation of the stress–strain curve and deviates substantially from the linear stress–strain relationship predicted by the other estimates.

Recall that all theoretical estimates are independent of the amplitude of the incident wave and therefore of the impact velocity. The effect of impact velocity only enters the problem in an indirect manner. SHPB experiments have shown that the striker impact velocity changes the frequency spectrum of the incident wave, i.e. the higher the loading velocity the higher the maximum frequency content. This is due to the circumstance that the contact surfaces at the striker/input bar interface are neither perfectly flat nor perfectly aligned in real experiments. As the error increases monotonically in ωt_s, a lower estimation accuracy is expected for higher impact velocities. The specimen length is another variable which enters the problem indirectly. Recall that the transit time t_s is proportional to the specimen length. Hence, based on the same argument as for the frequency content, we may conclude that the estimation error increases for longer specimens.

All conclusions regarding the quality of the stress–strain curve estimates are expected to hold true in both the elastic and plastic range of a dynamic experiment. It has been demonstrated that the use of the average strain in combination with either the average force based stress or output force based stress provides the best estimate of the stress–strain curve in the elastic case. In the plastic case, the variations of the stress and strain fields along the specimen axis are anticipated to be even smaller than in the elastic case. Consequently, we also recommend the direct estimates to approximate the stress–strain curve in the plastic case, while other methods should be used with care.

6. Conclusions

Different formulas have been proposed in the literature to estimate the stress–strain curve based on the forces and displacements at the boundary of a dynamically loaded specimen. A theoretical analysis is performed which makes use of the exact transient solution for a dynamically loaded elastic specimen. The results demonstrate that the so-called direct estimates, which are based on the force and displacement time histories at the specimen boundaries without artificial time shifts, provide the most accurate estimates of the stress–strain curve. Unless accurate input force measurements are available, the combination of the average strain with the output force based stress estimate is recommended for standard SHPB experiments.

Acknowledgements

DM and GG are grateful for the financial support of the French National Center for Scientific Research (CNRS). Thanks are due to Mr. Ionut Negreanu for performing the numerical simulations presented in this paper.

References

[1] Hopkinson B. A method of measuring the pressure in the deformation of high explosives by the impact of bullets. Phil Trans Roy Soc 1913;A213:437–52.
[2] Davies RM. A critical study of Hopkinson pressure bar. Phil Trans Roy Soc 1948;A240:375–457.
[3] Kolsky H. An investigation of the mechanical properties of materials at very high rates of loading. Proc Phys Soc (London) 1949;63:676–700.
[4] Harding J, Wood ED, Campbell JD. Tensile testing of materials at impact rate of strain. J Mech Eng Sci 1960;2:88–96.
[5] Duffy J, Campbell JD, Hawley RH. On the use of a torsional split Hopkinson bar to study rate effects in 1100-0 aluminium. J Appl Mech 1971;38:83–91.

[6] Yew EH, Chen CS. Experimental study of dispersive waves in beam and rod using FFT. J Appl Mech 1978;45:940–2.
[7] Follansbee PS, Franz C. Wave propagation in the split Hopkinson pressure bar. J Eng Mater Tech 1983;105:61–6.
[8] Gorham DA. A numerical method for the correction of dispersion in pressure bar signals. J Phys E: Sci Instrum 1983;16:477–9.
[9] Gamby D, Chaoufi J. Asymptotic analysis of wave propagation in a finite viscoelastic bar. Acta Mech 1991;87:163–78.
[10] Wang L, Labibes K, Azari Z, Pluvinage G. Generalization of split Hopkinson bar technique to use viscoelastic bars. Int J Impact Eng 1994;15:669–86.
[11] Zhao H, Gary G. On the use of SHPB technique to determine the dynamic behavior of the materials in the range of small strains. Int J Solids Struct 1996;33:3363–75.
[12] Liu Q, Subhash G. Characterization of viscoelastic properties of polymer bar using iterative deconvolution in the time domain. Mech Mater 2006;38:1105–17.
[13] Davies EDH, Hunter SC. The dynamic compression testing of solids by the method of the split Hopkinson pressure bar. J Mech Phys Solids 1963;11:155–79.
[14] Dharan CKH, Hauser FE. Determination of stress–strain characteristics at very high strain rates. Exp Mech 1970;10:370–6.
[15] Bertholf LD, Karnes J. Two-dimensional analysis of the split Hopkinson pressure bar system. J Mech Phys Solids 1975;23:1–19.
[16] Malinowski JZ, Klepaczko JR. Dynamic frictional effects as measured from the split Hopkinson bar. Int J Mech Sci 1986;28:381–91.
[17] Lindholm US. Some experiments with the split Hopkinson pressure bar. J Mech Phys Solids 1964;12:317–35.
[18] Conn AF. On the use of thin wafers to study dynamic properties of metals. J Mech Phys Solids 1965;13:311–27.
[19] Bell JF. An experimental diffraction grating study of the quasi-static hypothesis of the split Hopkinson bar experiment. J Mech Phys Solids 1966;14:309–27.
[20] Jahsman WE. Reexamination of the Kolsky technique for measuring dynamic material behavior. J Appl Mech 1971:77–82.
[21] Gray III GT. Classic split Hopkinson pressure bar testing. In: ASM Handbook, vol. 8. Mechanical Testing and Evaluation. Materials Park: OH; 2000. p. 462–76.
[22] Gary G, Rota L, Zhao H. Testing viscous soft materials at medium and high strain rates. In: Kawata K, Shiori J, editors. Constitutive relations in high/very high strain rates. Tokio: Springer-Verlag; 1996. p. 25–32.
[23] Zhao H, Gary G. A three-dimensional analytical solution of the longitudinal wave propagation in an infinite linear viscoelastic cylindrical bar. Application to experimental techniques. J Mech Phys Solids 1995;43:1335–48.
[24] Sogabe Y, Yokoyama T, Nakano M, Wu Z, Arimitsu Y. A viscoelastic split Hopkinson pressure technique and its applications to several materials. In: Chiba A, Tanimura S, Hokamatu K, editors. Impact engineering and application. London: Elsevier Science Ltd; 2001. p. 762–72.
[25] Sawas O, Brar NS, Brockman RA. Dynamic Characterization of compliant materials using an all-polymeric split Hopkinson bar. Exp Mech 1998;38:204–10.
[26] Gray III GT, Blumenthal WR. Split Hopkinson pressure bar testing of soft materials. In: ASM Handbook, vol. 8. Mechanical Testing and Evaluation. Materials Park: OH; 2000. p. 488–96.
[27] Ravichandran G, Subhash G. Split-Hopkinson pressure bar testing of ceramics. In: ASM handbook, vol. 8. Mechanical Testing and Evaluation. Materials Park: OH; 2000. p. 497–504.
[28] Song B, Chen W. Dynamic stress equilibrium in split Hopkinson pressure bar tests on soft materials. Exp Mech 2004;44(3):300–12.
[29] Mousavi S, Welch K, Valdek U, Lundberg B. Non-equilibrium split Hopkinson pressure bar procedure for non-parametric identification of complex modulus. Int J Impact Eng 2005;31:1133–51.
[30] Grolleau V, Gary G, Mohr D. Biaxial testing of sheet materials at high strain rates using viscoelastic bars. Exp Mech 2008;48(3):293–306.